# Simultaneous Tuning of Rotor Shape and Phase Current of Switched Reluctance Motors for Eliminating Input Current and Torque Ripples with Reduced Copper Loss

Kusumi Takayuki, Takuto Hara, Kazuhiro Umetani, Eiji Hiraki
Graduate School of Natural Science and Technology
Okayama University
Okayama, Japan

Published in: IEEE Transactions on Industry Applications
( Volume:)



DOI: 10.1109/TIA.2020.3015446

# Simultaneous Tuning of Rotor Shape and Phase Current of Switched Reluctance Motors for Eliminating Input Current and Torque Ripples with Reduced Copper Loss

Takayuki Kusumi, *Student Member, IEEE*, Takuto Hara, Kazuhiro Umetani, *Member, IEEE*, and Eiji Hiraki, *Member, IEEE*

***Abstract*—Switched reluctance motor (SRM) is recently emerging as a cost-effective but mechanically and thermally robust motor for vehicle propulsion. However, the conventional driving method of the SRM causes a large input current and torque ripples, both of which are scarcely acceptable for vehicle application. Recently, a promising driving method has been proposed that tunes the phase current to eliminate the input current and torque ripples simultaneously, although this method suffers from large copper loss when applied to the normal SRMs. To solve this problem, this paper proposes simultaneous tuning of the rotor shape in combination with the recently-proposed driving method, which includes only tuning of the phase current. Tuning of the rotor shape is targeted at minimizing the copper loss. Meanwhile, the stator structure is the same as the normal SRM design. The proposed approach was revealed to reduce the effective value of the phase current by 18% in simulation and by 23% in experiment compared with the recently-proposed driving method, without increasing the input current and torque ripples. This result suggests the effectiveness of tuning both the rotor shape and the phase current for applying SRMs to vehicle propulsion.**

***Index Terms*— Geometrical tuning, input-current ripple, phase-current waveform, rotor-shape, switched reluctance motors, torque ripple.**

## I. Introduction

RECENTLY, increasing CO2 emission is becoming a major environmental problem. In this context, the electrified vehicles such as the electric vehicles (EVs) and the hybrid vehicles (HVs) are emerging as a promising solution to this problem.

These electrified vehicles are commonly propelled by the interior permanent magnet synchronous motors (IPMSMs) to cover the wide variety of the operating condition in the output torque and the rotational speed. However, this motor significantly contains the permanent magnet, which is not only expensive but also mechanically fragile, and thermally degradable. Therefore, IPMSMs tend to lead to the significant cost-up of the electrified vehicles, and need special care for installation in the vehicle to protect IPSMs from the severe mechanical vibration during the vehicle travel and the limited cooling capability.

To overcome these difficulties, researchers are investigating the switched reluctance motor (SRM) as an alternative propulsion motor for the electrified vehicles. The SRM is a reluctance motor without the permanent magnets. Therefore, the SRM is beneficial in the cost-effectiveness as well as the mechanical and thermal robustness. Furthermore, the SRM is known to have the comparatively high power density among the reluctance motors [1]. All of these features are preferable for vehicular applications.

In contrast to these attractive features of the SRM, however, the SRM is reported to generate the large torque ripple as well as the large input current ripple [1][2]. The torque ripple leads to the noise vibration, thus deteriorating the driving comfort. The input current ripple, which is the ripple appearing in the DC power supply current to the inverter, leads to deterioration of the battery lifespan. Certainly, the input smoothing capacitor is commonly installed on the DC power supply to the inverter. However, this input smoothing capacitor generally can eliminate the high frequency current ripple generated by the switching operation of the inverter, although this capacitor cannot sufficiently eliminate the low frequency ripple generated in synchronization with the magnetization and demagnetization of the phase winding. Therefore, these two ripples are serious

Manuscript received December 30, 2019; revised May 13, 2020; accepted July 10, 2020. This work was supported in part by JSPS (JSPS KAKENHI Grant Number JP15K18021). This article was presented in part at IEEE Energy Conversion Congress and Exposition (ECCE2018), Portland, OR, USA, September 2018 [43].

Takayuki Kusumi is with Graduate School of Natural Science and Technology, Okayama University, 3-1-1 Tsushimanaka, Kita-Ku, Okayama, Japan. (e-mail: p75s6ovi@s.okayama-u.ac.jp)

Takuto Hara was with Graduate School of Natural Science and Technology, Okayama University, 3-1-1 Tsushimanaka, Kita-Ku, Okayama, Japan until March 2018. He is currently with FUJI ELECTRIC Co. Ltd., Mie, Japan, from April 2018. (e-mail: hara-takuto@fujielectric.com)

Kazuhiro Umetani was with Graduate School of Natural Science and Technology, Okayama University, 3-1-1 Tsushimanaka, Kita-Ku, Okayama, Japan, until March 2020. He is currently with Graduate School of Engineering, Tohoku University, 6-6-05 Aramaki-aza-aoba, Aoba-ku, Sendai, Miyagi, Japan, from April 2020. (e-mail: kazuhiro.umetani.e1@tohoku.ac.jp)

Eiji Hiraki is with the Graduate School of Natural Science and Technology, Okayama University, 3-1-1 Tsushimanaka, Kita-Ku, Okayama, Japan (e-mail: hiraki@okayama-u.ac.jp)

problems for applying the SRM to the vehicular propulsion.

To overcome these problems, a number of driving techniques have been proposed in literature. Particularly, the majority of these techniques only targets at the elimination of the torque ripple. For example, [3]-[23] have proposed the phase current waveforms that can reduce the torque ripple. Among them, [3]-[22] have derived their phase current waveforms by modifying the conventional square-shaped phase current waveforms using the torque sharing functions. In addition to the tuning of the phase-current waveform, [24]-[33] further incorporated the geometrical tuning of the rotor or stator shape to minimize the copper loss in addition to the reduction of the torque ripple. In these researches, the inductance profile was adjusted to reduce the phase current at the commutation to the next phase. Meanwhile, a few studies have been dedicated to the reduction of the input current ripple [34]-[38]. These studies have proposed their special inverter topologies in combination with the special control of these inverters, for driving the SRMs.

As can be seen above, these preceding studies [3]-[38] have proven their effectiveness in reducing either one of the torque and input current ripples. However, the vehicular application generally requires reduction in both of these two ripples. Therefore, the simultaneous reduction of the torque and input current ripples is important and is still a challenging issue.

To cast a new light on this issue, a promising driving technique has been proposed in [39][40]. This technique proposed a calculation method of the phase current waveform that can eliminate both of the input current and torque ripple based on the inductance profile of the SRM. This enabled elimination of these two ripples in SRMs with arbitrary inductance profile, including the commercially available SRMs. However, these studies have also reported that their phase current waveform resulted in the increase in the effective value by 58% [40], if applied to the normal SRM structure. This increase in the effective value of the phase current results in the copper loss approximately 2.5 times as large as that of the conventional square-shaped phase current waveform, which may cause difficulty in the heat dissipation from the propulsion motor by limited cooling equipment of the vehicle.

The power loss of the SRM is mainly classified into the copper loss and the core loss. However, [40] revealed that the phase flux waveform of this previous technique has smaller peak and the smoother shape than that of the conventional square-shaped phase current waveform, resulting in smaller changing rate of the phase flux with respect to the electric angle. Thereby, the core loss of this previous technique tends to be smaller than that of the conventional square-shaped phase current waveform. Consequently, the copper loss is the major problem of the previous technique, and therefore the practical application of this technique needs tuning of the SRM structure for reducing the copper loss.

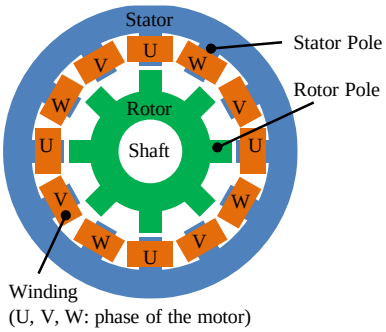

Fig. 1. Three-phase concentrated-winding SRM.

The purpose of this paper is to investigate effectiveness of simultaneous tuning of the SRM structure and the phase current waveform to reduce the input current and torque ripples with the minimum copper loss. In this paper, the tuning of the SRM structure is performed by searching for the rotor shape that implements the best possible inductance profile. Tuning of the phase current waveform and determination of the best inductance profile is based on the theory presented in [39][40], which is briefly reviewed in the next section.

This paper neglects the effect of the magnetic saturation, similarly as in [39][40], because the tuning method presented in this paper is based on this previous technique. This indicates that this paper also assumes that the SRM is used for propelling the vehicle traveling at moderate acceleration as in the city driving, similarly as [39][40]. In the vehicular application, the SRM should be designed to cover an instantaneous huge torque output for sudden acceleration or the hill start. Nonetheless, the SRM is commonly operated at a torque output far below the torque rating in the city driving. In fact, [41][42] reported that the propulsion motor is commonly operated at an output torque smaller than 1/3 of its maximum possible output torque in the new European driving cycle (NEDC) and JC08 driving cycle. Therefore, the SRM is assumed to output the torque far below the maximum rating and therefore the magnetization of the SRM is below the magnetic saturation level.

This paper is the updated version of the conference paper [43]. Compared with the conference paper, this paper further incorporates the detailed description of the derivation process for the inductance profile and the rotor shape. Additionally, this paper simulates the input current and torque ripples of the proposed technique under high rotational speed and large output torque in comparison with the conventional square-shaped phase current waveform drive and the previously proposed technique [39][40].

The remainder of this paper comprises 5 sections. Section II briefly reviews the previous technique [39][40], which is utilized for the tuning of the rotor shape and the phase current waveform. Section III discusses the tuning method of the rotor shape and the phase current waveform. Then, Section IV and section V presents the simulation and the experiment to validate the performance of the tuned SRM operated with the tuned phase current waveform. Finally, section VI gives the conclusions.

## II. Review of Derivation Method of Phase Current Waveform without Input Current and Torque Ripples

The previous studies [39][40] presented the calculation method of the phase current waveform that can eliminate both of the input current and torque ripples based on parameters characterizing the inductance profile. In these previous studies, these parameters are given based on the measurement of the inductance profile of the commercially available SRM, which

was utilized in the experiment. However, this paper seeks for the rotor shape that provides the best possible set of these parameters for minimizing the phase current. For this purpose, this section briefly reviews these previous studies.

Throughout this paper, the tuning method of the rotor shape and the phase current waveform is discussed for the three-phase concentrated-winding SRM as shown in Fig. 1. For simplifying the discussion, the following approximation is introduced: the mutual coupling between the phases is neglected similarly as in [39][40].

Derivation of the phase current waveform eliminating these two ripples is based on the analytical expression of the torque and the input current. For deriving this analytical expression, the total magnetic energy $E_{total}$ stored in the SRM is regarded as a function of the electrical angle and the magnetic flux of each phase winding. Because the magnetic coupling among the phase windings are neglected, $E_{total}$ can be expressed as

$$\begin{aligned} E_{total}(\theta_E,\varphi_U,\varphi_V,\varphi_W) &= E_U(\theta_E,\varphi_U)+E_V(\theta_E,\varphi_V) \\ &\quad + E_W(\theta_E,\varphi_W), \end{aligned} \tag{1}$$

where $E_U$, $E_V$, and $E_W$ are the magnetic energy contributed by phase U, V, and W, respectively; $\varphi_U$, $\varphi_V$, and $\varphi_W$ are the magnetic flux of a stator pole of phase U, V, and W, respectively; and $\theta_E$ is the electrical angle. The magnetic energy $E_J$ contributed by phase J can be expressed using the reluctance $R_J$ and the magnetic flux $\varphi_J$ of a stator pole of phase J. Because the magnetic saturation is not considered, $E_J$ is obtained as

$$E_J(\theta_E,\varphi_J)=\frac{P_s}{2}R_J(\theta_E)\varphi_J^2, \tag{2}$$

where $P_s$ is the number of the stator poles of phase J. The reluctance $R_J$ and the inductance $L_J$ of phase J has the following relation. Therefore, $R_J$ is the parameter that characterizes the inductance profile.

$$L_J(\theta_E)=\frac{N^2P_s}{R_J(\theta_E)}, \tag{3}$$

where $N$ is the number of turns of the phase winding on a stator pole.

The torque $\tau$ is expressed as the minus partial derivative of the total magnetic energy $E_{total}$ with respect to the mechanical angle [44]. Hence,

$$\begin{aligned} \tau(\theta_E,\varphi_U,\varphi_V,\varphi_W) &= -P_r\frac{\partial E_{total}(\theta_E,\varphi_U,\varphi_V,\varphi_W)}{\partial\theta_E} \\ &= -P_r\frac{\partial E_U(\theta_E,\varphi_U)}{\partial\theta_E}-P_r\frac{\partial E_V(\theta_E,\varphi_V)}{\partial\theta_E} \\ &\quad -P_r\frac{\partial E_W(\theta_E,\varphi_W)}{\partial\theta_E}, \end{aligned} \tag{4}$$

where $P_r$ is the number of rotor poles.

The input current $i_E$ can be expressed as the sum of the effective power supplied to the SRM divided by the voltage of the DC power supply to the inverter. Because the phase current $i_J$ and the inverter output voltage $v_J$ of phase J can be expressed as

$$i_J=\frac{\partial E_J(\theta_E,\varphi_J)}{NP_s\partial\varphi_J},\quad v_J=NP_s\frac{d\varphi_J}{dt}=NP_s\Omega P_r\frac{d\varphi_J}{d\theta_E}, \tag{5}$$

where $\Omega$ is the angular velocity of the rotor, $i_E$ is expressed as

$$\begin{aligned} i_E &= \frac{1}{V_{DC}}(i_Uv_U+i_Vv_V+i_Wv_W) \\ &= \frac{\Omega P_r}{V_{DC}}\left(\frac{\partial E_U(\theta_E,\varphi_U)}{\partial\varphi_U}\frac{d\varphi_U}{d\theta_E}\right. \\ &\quad \left.+\frac{\partial E_V(\theta_E,\varphi_V)}{\partial\varphi_V}\frac{d\varphi_V}{d\theta_E}+\frac{\partial E_W(\theta_E,\varphi_W)}{\partial\varphi_W}\frac{d\varphi_W}{d\theta_E}\right), \end{aligned} \tag{6}$$

where $V_{DC}$ is the voltage of the DC power supply. Noting $\partial E_U/\partial\varphi_U\cdot d\varphi_U/d\theta_E$ can be expressed as

$$\frac{\partial E_U(\theta_E,\varphi_U)}{\partial\varphi_U}\frac{d\varphi_U}{d\theta_E}=\frac{dE_U}{d\theta_E}-\frac{\partial E_U}{\partial\theta_E}, \tag{7}$$

(6) can be rewritten as

$$\begin{aligned} i_E &= \frac{\Omega P_r}{V_{DC}}\left(\frac{dE_U}{d\theta_E}-\frac{\partial E_U}{\partial\theta_E}\right. \\ &\quad \left.+\frac{dE_V}{d\theta_E}-\frac{\partial E_V}{\partial\theta_E}+\frac{dE_W}{d\theta_E}-\frac{\partial E_W}{\partial\theta_E}\right) \\ &= \frac{\Omega P_r}{V_{DC}}\left(\frac{dE_U}{d\theta_E}+\frac{dE_V}{d\theta_E}+\frac{dE_W}{d\theta_E}+\frac{\tau}{P_r}\right). \end{aligned} \tag{8}$$

Now, the phase current that can eliminate both of the input current and torque ripples can be analytically derived based on these equations. As in many practical SRM drive methods, this paper also assumes that the phase current of each phase is symmetrical. Consequently, the magnetic flux of each phase, i.e. $\varphi_U$, $\varphi_V$, and $\varphi_W$, is also symmetrical because of the symmetry among $i_U$, $i_V$, and $i_W$ as well as the symmetry of the reluctance among the phases. Therefore, this section hereafter regards the phase current and the magnetic flux of phase $U$ as functions of $\theta_E$ and express the input current and torque by these functions, thus determining the function of $i_U$ that can eliminate both of the input current and torque ripples. (Hence, the phase current $i_V$, and $i_W$ are obtained by $i_V(\theta_E)=i_U(\theta_E+4/3\pi)$ and $i_W(\theta_E)=i_U(\theta_E+2/3\pi)$.)

Because of the symmetry among the phases, substituting (2) into (4) and (8) yields

$$\tau = -\frac{P_rP_s}{2}\left\{f(\theta_E)+f\left(\theta_E+\frac{4\pi}{3}\right)+f\left(\theta_E+\frac{2\pi}{3}\right)\right\}, \tag{9}$$

$$\begin{aligned} i_E &= \frac{\Omega P_r}{V_{DC}}\left(\frac{P_s}{2}\frac{dR_U\varphi_U^2}{d\theta_E}+\frac{P_s}{2}\frac{dR_V\varphi_V^2}{d\theta_E}\right. \\ &\quad \left.+\frac{P_s}{2}\frac{dR_W\varphi_W^2}{d\theta_E}+\frac{\tau}{P_r}\right) \\ &= \frac{\Omega P_r}{2V_{DC}}\left\{\frac{d}{d\theta_E}g(\theta_E)+\frac{d}{d\theta_E}g\left(\theta_E+\frac{4}{3}\pi\right)\right. \\ &\quad +\frac{d}{d\theta_E}g\left(\theta_E+\frac{2}{3}\pi\right)-P_sf(\theta_E) \\ &\quad \left.-P_sf\left(\theta_E+\frac{4}{3}\pi\right)-P_sf\left(\theta_E+\frac{2}{3}\pi\right)\right\}, \end{aligned} \tag{10}$$

where $g(\theta_E)$ and $f(\theta_E)$ are the function of the electric angle $\theta_E$ defined as

$$g(\theta_E) = 2E_U = P_s R_U \varphi_U^2, \tag{11}$$

$$f(\theta_E) = \frac{\partial R_U}{\partial \theta_E}\varphi_U^2 = \frac{g(\theta_E)}{P_s}\frac{\partial}{\partial \theta_E}\ln R_U. \tag{12}$$

$g(\theta_E)$ and $f(\theta_E)$ are regarded not as the functions of $\theta_E$ and $\varphi_U$ but as the functions only of $\theta_E$ because $\varphi_U$ is regarded to be the function of $\theta_E$ similarly as $R_U$.

As can be seen in (9) and (10), the necessary and sufficient condition for eliminating both of the input current ripple and the torque ripple is that both of $f(\theta_E)$ and $g(\theta_E)$ do not contain the harmonics of multiples of three. Once such a pair of $f(\theta_E)$ and $g(\theta_E)$ is determined, the phase current waveform can be readily calculated as

$$i_U(\theta_E) = \frac{R_U \varphi_U}{N} = \sqrt{\frac{R_U g(\theta_E)}{N^2 P_s}}. \tag{13}$$

Next, the pair of $f(\theta_E)$ and $g(\theta_E)$ that does not contain the harmonics of multiples of three is determined based on the given reluctance profile $R_U(\theta_E)$. For this purpose, $R_U(\theta_E)$ is approximated to have the following form:

$$\begin{aligned}\ln R_U(\theta_E) = {} & K_0 - K_1\cos\theta_E - K_2\cos 2\theta_E \\ & - K_3\cos 3\theta_E - K_4\cos 4\theta_E - K_5\cos 5\theta_E.\end{aligned} \tag{14}$$

(The origin of $\theta_E$ is defined as the aligned position of phase U.) The parameters $K_0$–$K_5$ can be easily determined by Fourier's expansion of $\ln R_U(\theta_E)$.

Similarly, $g(\theta_E)$ is assumed not to contain high order harmonics of $\theta_E$ as well as the harmonics of multiples of three. Then, $g(\theta_E)$ can be expressed by the following form:

$$\begin{aligned}g(\theta_E) = P_s\{ & A_0 + A_1\sin\theta_E + A_2\sin 2\theta_E \\ & + A_4\sin 4\theta_E + A_5\sin 5\theta_E + B_1\cos\theta_E \\ & + B_2\cos 2\theta_E + B_4\cos 4\theta_E + B_5\cos 5\theta_E\},\end{aligned} \tag{15}$$

The solution of $f(\theta_E)$ can be obtained by substituting (14) and (15) into (12). Therefore, from the requirement that $f(\theta_E)$ should not contain the harmonics of multiples of three, the conditions of parameters $A_0$–$A_5$ and $B_1$–$B_5$, under which both of $f(\theta_E)$ and $g(\theta_E)$ do not contain the harmonics of multiples of three, can be formulated. Consequently, $A_0$–$A_5$ and $B_1$–$B_5$ are obtained as

$$A_4 = \frac{-\{k_4 - k_2 + (k_1 - k_5)k_5/k_4\}A_1}{(k_1 - k_5)(k_2/k_4 - k_1k_5/k_4^2) + k_1 - k_2k_5/k_4}, \tag{16}$$

$$A_2 = -(k_5/k_4)A_1 - (k_2/k_4 - k_1k_5/k_4^2)A_4, \tag{17}$$

$$B_4 = \frac{2k_3A_0 + \{k_4 + k_2 - (k_1 + k_5)k_5/k_4\}B_1}{(k_1 + k_5)(k_2/k_4 - k_1k_5/k_4^2) + k_1 - k_2k_5/k_4}, \tag{18}$$

$$B_2 = -(k_5/k_4)B_1 - (k_2/k_4 - k_1k_5/k_4^2)B_4, \tag{19}$$

$$A_5 = -(k_5/k_4)A_4, \quad B_5 = -(k_5/k_4)B_4, \tag{20}$$

where $k_1$–$k_5$ are defined as

$$\begin{aligned}&k_1 = K_1, \quad k_2 = 2K_2, \quad k_3 = 3K_3, \\ &k_4 = 4K_4, \quad k_5 = 5K_5.\end{aligned} \tag{21}$$

As can be seen in (16)–(20), the set of parameters $A_0$–$A_5$ and $B_1$–$B_5$ can be obtained from an arbitrary set of parameters $K_0$–$K_5$, which characterizes the inductance profile. Furthermore, there are infinitely large number of sets of $A_0$–$A_5$ and $B_1$–$B_5$ that satisfy these conditions. (However, $A_0$ is required be chosen so that $g(\theta_E)$ is always greater than zero because of (11).) Once such a set of $A_0$–$A_5$ and $B_1$–$B_5$ is determined, the phase current can be readily derived using (15) and (13). Therefore, there are infinitely large number of the phase current waveforms that can simultaneously eliminate the input current and torque ripples for an arbitrary inductance profile.

## III. Tuning of Rotor Shape and Phase Current Waveform

### A. Overview of Tuning Method

The previous section derived the phase current waveform that can eliminate the input current and torque ripples based on the given parameters of the inductance profile, i.e. $K_0$–$K_5$. However, parameters $K_0$–$K_5$ can be rather regarded to be also flexible, similarly as $A_0$–$A_5$ and $B_1$–$B_5$. Therefore, this section searches for the improved set of the parameters $K_0$–$K_5$, $A_0$–$A_5$, and $B_1$–$B_5$ that eliminates the input current and torque ripples with minimum effective value of the phase current and determine the rotor shape that implements the tuned parameters of $K_0$–$K_5$ as well as the phase current that implements the tuned parameters of $A_0$–$A_5$ and $B_1$–$B_5$.

However, it is worth noticing that not any set of $K_0$–$K_5$, i.e. the parameters of the inductance profile, can be implemented in a rotor shape due to the geometrical and mechanical restrictions of the rotor, such as the dimensions and the minimum gap. Therefore, this section considers the commercially available SRM, whose specifications are shown in Table I, and search for the improved rotor shape under the same restriction as the rotor of this SRM. Thus, the resultant rotor shape and phase current waveform corresponds to the tuned rotor shape and phase current waveform that can be achieved by modifying the rotor shape without changing the stator.

This SRM under consideration has smaller power rating than the SRM for EV propulsion. The reason is that the experiment was also carried out in section V to test the tuning result of this section. Because of the limitation of the testing equipment for the motor test bench, the experiment must be carried out with a downsized motor. Consequently, the SRM under consideration has a power rating of 1.2kW with the maximum voltage of 96V.

The geometrical and mechanical restriction of the rotor is difficult to formulate as a restriction on the inductance profile; and therefore, it is difficult to infer the possible range of $K_0$–$K_5$. To overcome this difficulty, the following numerical searching approach was adopted for tuning the rotor shape and the phase current waveform.

The overall tuning procedure is presented in Fig. 2. The first step parameterized features of the inductance profile and introduced the restriction that these parameters should take specific values. These values are initially given the same values as the original SRM before tuning. The second step determined the best set of $K_0$–$K_5$, $A_0$–$A_5$, and $B_1$–$B_5$ that minimizes the effective value of the phase current waveform under this restriction. As a result, we obtained the best pair of the inductance profile and the phase current waveform. In the third

step, the finite-element-method (FEM) analysis was carried out to search for the rotor shape that implements the determined inductance profile. If the FEM analysis failed to find the appropriate rotor shape that achieves the determined inductance profile, the values assigned for the restrictions on the inductance profile were changed, unless the practically possible best value is apparent. Then, the aforementioned procedure was repeated until the appropriate rotor shape was found. Finally, after the appropriate rotor shape was found, $K_0$–$K_5$ were extracted from the inductance profile of the SRM with this appropriate rotor shape, which is determined by measurement of the prototype SRM or the FEM analysis. Then, $A_0$–$A_5$ and $B_1$–$B_5$ were determined again so that these parameters eliminate the input current and torque ripples with minimum effective value of the phase current, thus resulting in the phase current waveform for the tuned rotor shape.

### *B. Set Restriction on Inductance Profile*

The geometrical and mechanical restriction of the rotor shape limits the possible inductance profile. For formulating this restriction on the inductance profile, the maximum inductance $L_{max}$ and the minimum inductance $L_{min}$ were adopted as the two parameters that characterizes this restriction. These two parameters are closely and straightforwardly related to parameters $K_0$–$K_5$, because the following relation can be obtained according to (14):

$$L_{\max} = \frac{N^2 P_s}{\exp\left(K_0 - K_1 - K_2 - K_3 - K_4 - K_5\right)}. \quad (22)$$

$$L_{\min} = \frac{N^2 P_s}{\exp\left(K_0 + K_1 - K_2 + K_3 - K_4 + K_5\right)}. \quad (23)$$

The commercially available SRM is commonly designed to have its maximum inductance $L_{max}$ as large as possible to generate sufficient magnetic flux with small phase current. Furthermore, the minimum inductance $L_{min}$ is also commonly designed to be as small as possible for maximizing $L_{max}$–$L_{min}$ because large value of $L_{max}$–$L_{min}$ is effective to generate large torque output [3].

Therefore, $L_{max}$ and $L_{min}$ are first imposed to have the same value as the SRM shown in Table I. However, search for the improved rotor shape under this requirement can be failed. In this case, the value imposed on $L_{min}$ is gradually increased, while keeping the value imposed on $L_{max}$ unchanged.

The reason why the value of $L_{max}$ is unchanged is that the output torque $\tau$ is not affected by the DC offset in the reluctance profile because the output torque $\tau$ is only dependent on the partial derivative of the reluctance profile $R_U$ according to (9) and (12). Therefore, the minimum DC offset in the reluctance profile is preferable to minimize the necessary phase current for generating sufficient magnetic flux. This indicates that $L_{max}$ should be the maximum possible value, which equals to $L_{max}$ of the original SRM shown in Table I.

### *C. Tuning of Inductance Profile and Phase Current Waveform*

Under the aforementioned restriction on the inductance profile, this subsection searches for the set of parameters $K_0$–$K_5$, $A_0$–$A_5$, and $B_1$–$B_5$ that satisfy (16)–(20) and the requirement of $g(\theta_E)\geq 0$, i.e. conditions to eliminate both of the input current and torque ripples, with the minimum effective value of the phase current waveform. For this purpose, the effective value of the phase current waveform should be compared under the same average torque output of 1 N·m. (The tuned set of parameters is independent of the output torque because the magnetic saturation is neglected.) Hence, the following relation was further imposed:

$$\tau_{av} = \frac{3P_r P_s}{4}\left(5A_5K_5 + 4A_4K_4 + 2A_2K_2 + A_1K_1\right) = 1\ \mathrm{N\cdot m}, \quad (24)$$

where $\tau_{av}$ is the average torque, and searched for the improved set of $K_0$–$K_5$, $A_0$–$A_5$, and $B_1$–$B_5$ that yields the phase current waveform with minimum effective value. Consequently, all the required conditions for searching for improved set of $K_0$–$K_5$, $A_0$–$A_5$, and $B_1$–$B_5$ was summarized in Table II.

TABLE I
SPECIFICATIONS OF SRM CONSIDERED FOR TUNING

| | |
|---|---|
| Model number | RB165SR-96CSRM |
| | (Motion System Tech. Inc.) |
| Rate value | 1.2 kW, 96 V, 6000 rpm |
| Structure | Stator: 12 poles, Rotor: 8 poles, |
| | Number of turns: 14 tunes/pole |
| | Outer diameter of stator: 136 mm |
| | Outer diameter of rotor: 83 mm |
| | Gap between stator and rotor: 0.3 mm |
| | Diameter of shaft: 25 mm |
| | Stack length: 40 mm |
| Material | 35H300 (Nippon Steel Corp.) |
| Characteristics | Maximum reluctance $R_{max}$: $4.1\times10^6$ A/Wb |
| | (Minimum inductance: 0.2 mH) |
| | Minimum reluctance $R_{min}$: $0.5\times10^6$ A/Wb |
| | (Maximum inductance: 1.5 mH) |

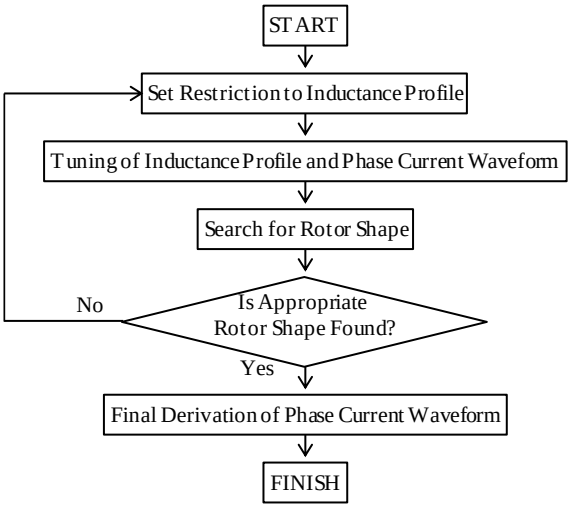


Fig. 2. Flow chart for tuning the rotor shape and the phase current waveform.

TABLE II
CONDITION IMPOSED FOR PARAMETER TUNING

| | |
|---|---|
| Maximum Inductance | $L_{max}$ = 1.5 mH |
| Minimum Inductance | $L_{min}$ = 0.2 mH at the first time of tuning. |
| | Gradually increased after |
| | the 2nd time of tuning |
| Output Torque | $\tau$ = 1Nm |
| Function | $g(\theta_E)\geq 0$ |
| Equation | (16)–(20) |

These parameters were tuned by the brute-force search by changing $K_2$ and $K_3$ by the step of $2\times10^{-3}$, $K_4$ by the step of $1\times10^{-3}$, $K_5$ by the step of $5\times10^{-4}$, $A_0$ and $B_1$ by the step of $1\times10^{-3}$. The other parameters are automatically determined according to (16)–(20) as well as the imposed conditions listed in Table II.

As an example, Fig. 3 shows the inductance profile $L_U$ and the reluctance profile $R_U$ of the tuning result when the restriction on the inductance profile requested that $L_{max}$ and $L_{min}$ were set at the same values as the original SRM. Figure 3 also shows $L_U$ and $R_U$ of the original SRM shown in Table I.

In addition, Figure 4 shows the phase current waveform $i_U$ and the magnetic flux waveform $\varphi_U$ of the tuning result in comparison with those of the conventional square-shaped phase current waveform, and those of the previous technique, in which only $A_0$–$A_5$ and $B_1$–$B_5$ was tuned to minimize the effective value of the phase current without tuning the inductance profile. (The firing and extinction angles of the conventional square-shaped phase current waveform was set at 208 and 352 degrees, respectively, where the torque ripple is minimized in the SRM under consideration at the rotational speed of 125 r/min. For the phase current waveform of the previous technique, the parameters are determined by the brute-force search by changing $A_0$ and $B_1$ by steps of $1\times10^{-4}$ under the requirement of (16)–(20), $g(\theta_E)\geq0$, and $\tau_{av}$=1 N·m.)

As can be seen in Fig. 3 and Fig. 4, the tuning of parameters $K_0$–$K_5$, $A_0$–$A_5$, and $B_1$–$B_5$ resulted in a great difference in the inductance profile as well as the phase current waveform.

### *D. Search for Rotor Shape*

This subsection searches for the rotor shape that approximately achieves the tuned inductance profile represented by the tuned parameters $K_0$–$K_5$, obtained in the previous subsection. The search of the rotor shape was performed by modifying the original rotor shape, shown in Fig. 5(a), of the commercially available SRM of Table I. For this purpose, the 2 dimensional FEM analysis was utilized with JMAG-Designer14.1 (JSOL Crop.) software to calculate the inductance profile from the rotor shape. The materials used in the FEM analysis SRM model are listed in Table III. This FEM analysis model incorporates the magnetic saturation but does not incorporate the iron loss. The inductance profile was calculated at a sufficiently small magnetization below the magnetic saturation.

The rotor shape was determined by the manual trial-and-error approach using the FEM software. However, there are infinitely large number of the possible rotor shapes; the trial-and-error approach can scarcely determine the rotor shape if the candidates of the rotor shape are not limited by introducing a few parameters that define the rotor shape. Consequently, the following four parameters are introduced for the search for the rotor shape: $\theta_{r1}$, $\theta_{r2}$, $w_{r1}$, and $w_{r2}$.

These four parameters are chosen because they are supposed to have an essential effect on the prominent features of the tuned inductance (or reluctance profile).

As can be seen in Fig. 3(b), the tuned reluctance profile has smaller reluctance than the original reluctance profile at a wide range of the electrical angle. This feature needs the shallow valley of the rotor shape, as shown in Fig. 5(b), because the reluctance is proportional to the gap between the stator pole and the rotor surface in a rough approximation. For simply expressing the shape of the shallow valley, the pole width $w_{r2}$ and the angle $\theta_{r1}$ of the shallow valley are introduce as defined in Fig. 5(b).

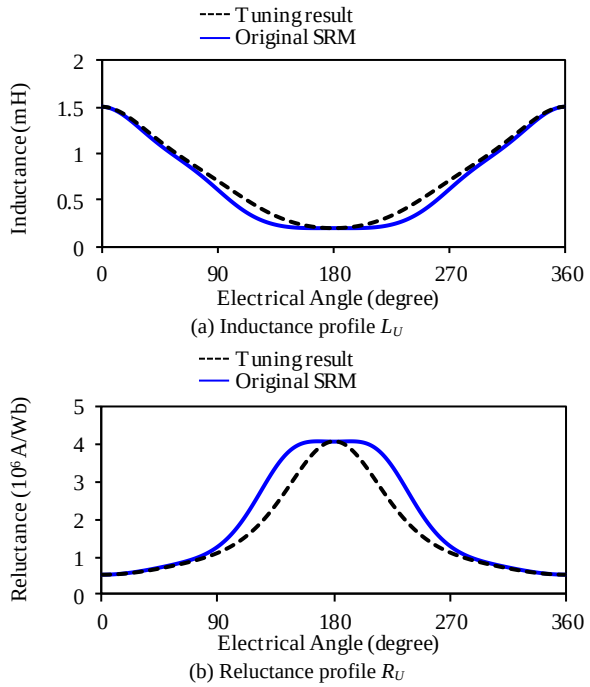


(a) Inductance profile $L_U$

(b) Reluctance profile $R_U$

Fig. 3. Inductance profile $L_U$ and reluctance profile $R_U$ of the tuning result in comparison with that of the original SRM shown in Table II.

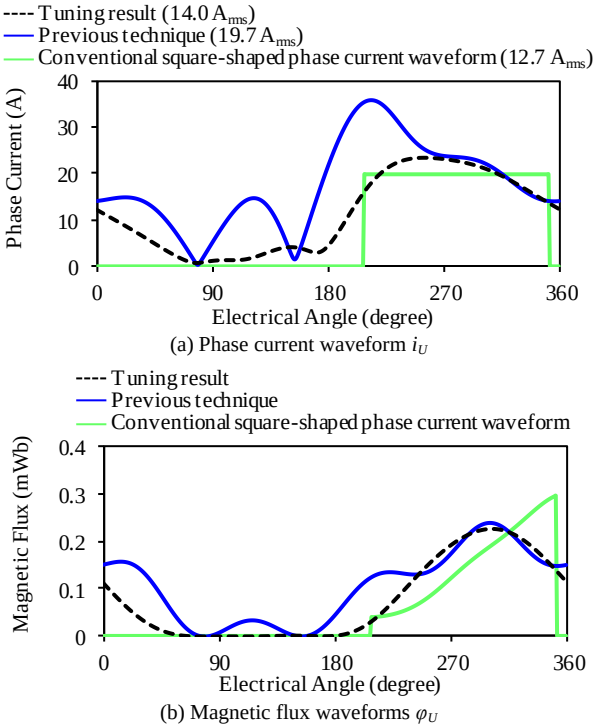


(a) Phase current waveform $i_U$

(b) Magnetic flux waveforms $\varphi_U$

Fig. 4. Phase current waveform $i_U$ and magnetic flux waveform $\varphi_U$ of tuning result in comparison with those of conventional square-shaped phase current waveform and those of the previous technique in which only the phase current was tuned.

TABLE III
MATERIAL USED IN FEM ANALYSIS MODEL

| Component | Material name or relative magnetic permeability |
|---|---|
| Stator | Material name: 35H300 (Nippon Steel Corp.) |
| Rotor | Material name: 35H300 (Nippon Steel Corp.) |
| Winding | Relative magnetic permeability: 1 |
| Shaft | Relative magnetic permeability: 1 |

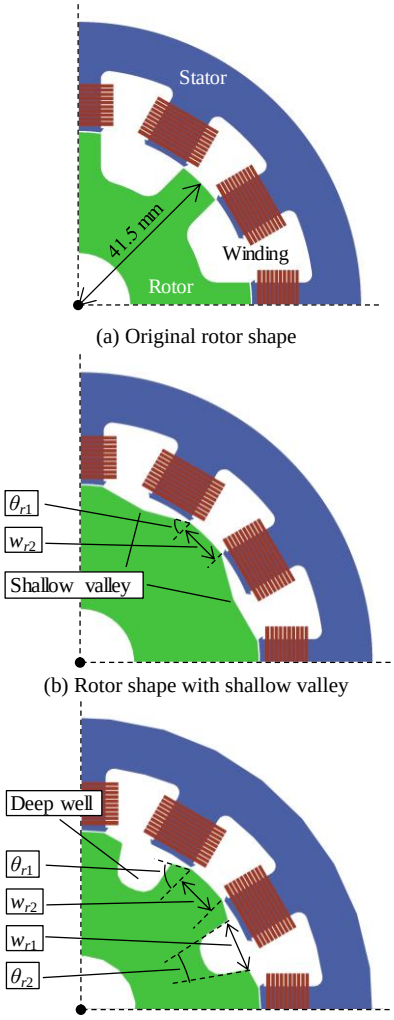


(a) Original rotor shape

(b) Rotor shape with shallow valley

(c) Basic shape assumed for search for rotor shape

Fig. 5. Basic rotor shape and parameters used for rotor shape searching process.

Nonetheless, the tuned reluctance profile has a sharp peak at the unaligned position. Therefore, the gap between the stator pole and the rotor surface should become suddenly large near the unaligned position. For this purpose, the deep well was further made on the shallow valley near the unaligned positon, as shown in Fig. 5(c). Therefore, the well width $w_{r1}$ and the well taper angle $\theta_{r2}$ are introduced to parameterize the shape of the well, as defined in Fig. 5(c).

However, in spite of the effort to adjust these four parameters, the minimum of the inductance profile (or the peak of the reluctance profile) is often difficult to be achieved by the rotor shape. The reason is that the deep well inevitably has the narrower width than the dip on the original rotor shape, and therefore the resultant inductance profile has a larger minimum (or the resultant reluctance profile has a smaller peak) than the original rotor shape. Therefore, if adjustment of these four parameters failed to satisfy the tuned inductance profile at the unaligned position, the value assigned to $L_{min}$, which is the condition given to determine the tuned inductance profile, was increased and the whole procedure described in subsections *B*–*D* was repeated again until the rotor shape can satisfy the tuned inductance profile determined in subsection *C*.

### *E. Final Derivation of Phase Current Waveform*

After tuning the rotor shape in the previous subsection, the phase current waveform for the rotor shape was finally derived. For this purpose, parameters $K_0$–$K_5$ were extracted from the inductance profile, measured on the prototype SRM with the tuned rotor shape, and searched for parameters $A_0$–$A_5$, and $B_1$–$B_5$ that satisfy (16)–(20) and the requirement of $g(\theta_E)\geq 0$, i.e. conditions to eliminate both of the input current and torque ripples, with the minimum effective value of the phase current waveform at the torque output of 1 N·m.

These parameters were tuned by the brute-force search by changing $A_0$ and $B_1$ by the step of $1\times10^{-4}$. The other parameters are automatically determined according to (16)–(20) and (24).

However, in the simulation-based performance evaluation made in the next subsection and the next section, there is no actual prototype of the SRM. Therefore, parameters $K_0$–$K_5$ extracted from the inductance profile calculated by the FEM simulation were utilized, instead of the experimentally measured inductance profile of the prototype SRM.

### *F. Result of Tuning*

As a result of the aforementioned procedure, the tuned rotor shape and the tuned phase current profile was finally obtained. Figure 6 shows the inductance profile and the reluctance profile of the tuned rotor shape in comparison with those of the original rotor shape. Figure 7 shows the tuned phase current waveform and its magnetic flux waveform in comparison with those of the conventional square-shaped phase current waveform and those of the previous technique, in which only $A_0$–$A_5$ and $B_1$–$B_5$ was tuned for the original rotor shape [39][40]. Both of the conventional square-shaped phase current waveform and the previous technique uses the original rotor shape. Figure 8 shows the tuned rotor shape. Tables IV and V list the values of parameters $\theta_{r1}$, $\theta_{r2}$, $w_{r1}$, and $w_{r2}$, used in the tuning of the rotor shape, and the values of parameters $K_0$–$K_5$, $A_0$–$A_5$, and $B_1$–$B_5$, determined by the final derivation of the phase current. (The firing and extinction angles of the conventional square-shaped phase current waveform was set at 208 and 352 degrees, respectively, where the torque ripple is minimized at the rotational speed of 75 r/min. For the phase current waveform of the previous technique, the parameters are determined by the brute-force search by changing $A_0$ and $B_1$ by steps of $1\times10^{-4}$.)

As can be seen in the figure, the tuning result has smaller phase current at a wide range of the electrical angle. The tuning result reduced the effective value of the phase current by 18 % in comparison with the previous technique [39][40], which corresponds to the reduction in the copper loss by 32 %. Certainly, the tuning result exhibited the phase current larger than the conventional square-shaped waveform by 28 %, which

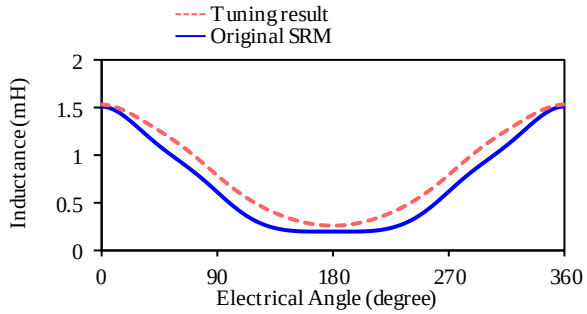


(a) Inductance profile $L_U$

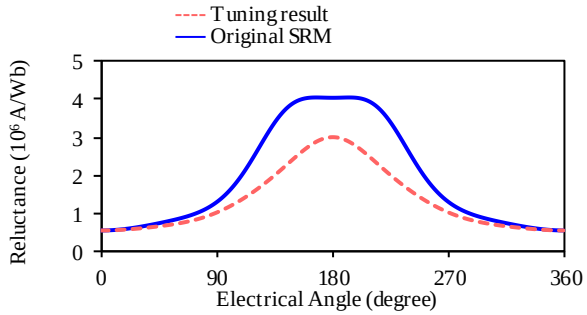


(b) Reluctance profile $R_U$

Fig. 6. Inductance profile $L_U$ and reluctance profile $R_U$ of the original rotor and the tuning result.

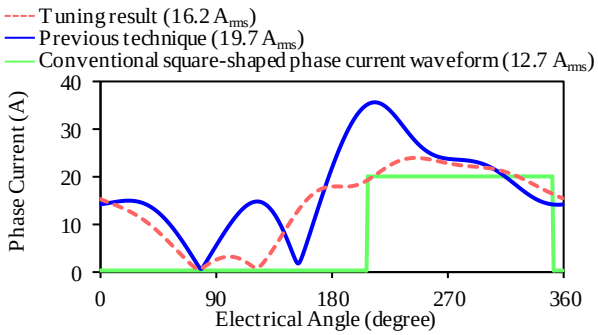


(a) Phase current waveform $i_U$

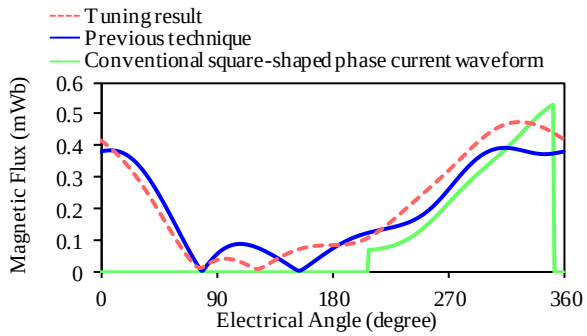


(b) Magnetic flux waveform $\varphi_U$

Fig. 7. Phase current waveform $i_U$ and magnetic flux waveform $\varphi_U$ of tuning result, the previous technique, and conventional square-shaped phase current waveform for outputting the average torque of 1 N·m.

corresponds to the increase in the copper loss by 62 %. However, unlike the conventional square-shaped waveform, the phase current of the tuning result can eliminate both of the input current and torque ripples, which is essential for application to vehicle propulsion.

Furthermore, the magnetic flux waveform of the tuning result is smoother and has slightly smaller peak than the conventional

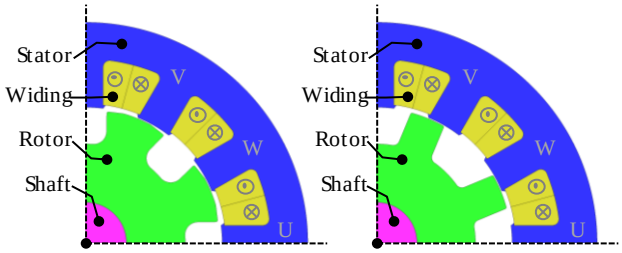


(a) Tuning result (b) Original rotor shape

Fig. 8. Tuning result of the rotor shape in comparison with the original rotor shape.

TABLE IV
PARAMETERS DETERMINED FOR ROTOR SHAPE

| Parameter | Tuning result | Original rotor shape |
|---|---|---|
| $\theta_{r1}$ | 74.4 degrees | - |
| $\theta_{r2}$ | 1.1 degrees | 45.0 degrees |
| $w_{r1}$ | 13.0 mm | 21.46 mm |
| $w_{r2}$ | 9.0 mm | 10.86 mm |

TABLE V
TUNED PARAMETERS FOR ROTOR SHAPE AND PHASE CURRENT WAVEFORM

| | | | | | |
|---|---|---|---|---|---|
| $K_0$ | 13.916 | $A_0$ | $5.33\times10^{-2}$ J | $B_1$ | $3.64\times10^{-2}$ J |
| $K_1$ | 0.849 | $A_1$ | $-5.38\times10^{-2}$ J | $B_2$ | $1.70\times10^{-3}$ J |
| $K_2$ | −0.112 | $A_2$ | $-1.69\times10^{-2}$ J | $B_4$ | $2.66\times10^{-4}$ J |
| $K_3$ | 0.022 | $A_4$ | $-4.07\times10^{-4}$ J | $B_5$ | $-2.08\times10^{-3}$ J |
| $K_4$ | 0.002 | $A_5$ | $3.19\times10^{-3}$ J | | |
| $K_5$ | 0.010 | | | | |

The values of $K_0$-$K_5$ are obtained by applying the natural logarithm to the value of $R_U(\theta_E)$ expressed in the unit of A/Wb.

square-shaped phase current waveform, similarly as the previous technique. This indicates that the tuning result can operate at higher rotational speed as well as the higher output torque below the magnetic saturation than the conventional square-shaped phase current waveform.

The maximum output torque of the SRMs is difficult to be clearly defined because the SRMs are often driven at the magnetization beyond the magnetic saturation level when the instantaneous large torque output is required. However, according to Fig. 7, the peak magnetic flux of the tuning result, the previous technique and the conventional square-shaped phase current waveform was 0.48mWb, 039mWb, and 0.53mWb, respectively, at the torque output of 1 N·m. Therefore, the peak magnetic flux of these three techniques takes similar values. This suggests that the proposed technique has similar maximum output torque as the previous technique and the conventional square-shaped phase current waveform because the magnetization reaches the magnetic saturation level at similar output torque.

Certainly, as can be seen in Fig. 8, the tuning results increased the iron mass of the rotor. As a result of the tuning, the cross-sectional area of the rotor increased by 12 %, which indicates the increase in the iron mass of the rotor by 12 %. In this sense, the proposed technique led to the increase in the material cost of the iron. However, the total increase in the iron mass including the rotor and the stator was within 4 %, which may not be a significant increase in the material cost.

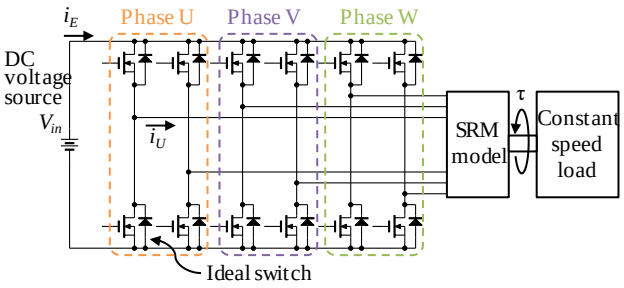


Fig. 9. Three-phase H-bridge inverter employed for simulation.

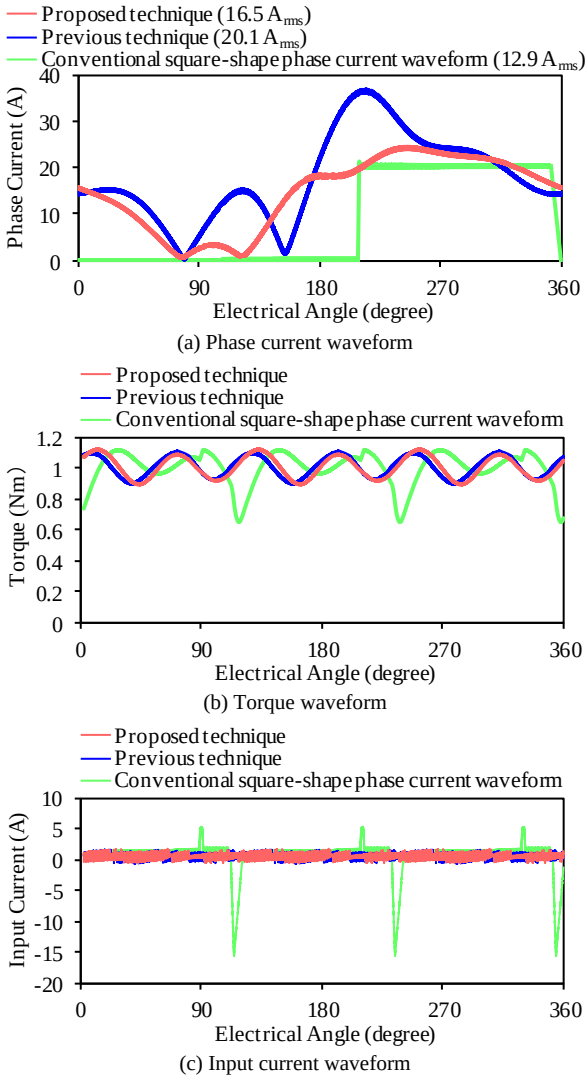


Fig. 10. Simulation result of the SRM operated at the rotational speed of 500 r/min and the output torque of 1 N·m. The effective values of the phase current are presented in the legend of Fig. 10(a).

Consequently, the simultaneous tuning of the rotor shape and the phase current waveform resulted in elimination of the input current and torque ripples with smaller copper loss than the previous technique.

## IV. Simulation

The simulation was carried out to verify the effectiveness of the tuning result of the rotor shape and the phase current waveform obtained in the previous section. In this simulation, the input current and torque ripples of the tuned phase current waveform with the tuned rotor shape, i.e. the proposed technique, are evaluated and compared with the two phase current waveforms with the original rotor shape, i.e. the conventional square-shaped phase current waveform and the previous technique, in which only the phase current was tuned based on the original rotor shape.

Hereafter, the input current ripple ratio $i_{E\_ripple}$ and the torque ratio $\tau_{ripple}$ are defined as the half of the peak-to-peak value normalized by the average value. Hence,

$$i_{E\_ripple} = \frac{i_{E\_PP}}{2i_{E\_av}}, \quad \tau_{ripple} = \frac{\tau_{PP}}{2\tau_{av}}, \tag{25}$$

where $\tau_{PP}$ and $i_{E\_PP}$ are the peak-to-peak values of the torque and input current waveforms, and $\tau_{av}$ and $i_{E\_av}$ are the average value obtained from the torque and input-current waveforms. Note that $\tau_{PP}$ and $i_{E\_PP}$ are obtained after the moving average process which decouples the ripples generated by the inverter switching.

Figure 9 shows the simulation model. The whole simulation model was constructed in the circuit simulator PSIM11.1 (Myway Corp.) The SRM model was constructed according to the modeling method presented in [44] as a behavioral model based on the magnetic co-energy dependence on the electric angle and the magnetic flux linkage of the phase windings. This behavioral model does not contain the mechanical loss, the iron loss, and the copper loss, although the model contains the effect of the magnetic saturation. The magnetic co-energy dependence, used for the behavioral model, was calculated by the two dimensional FEM analysis using JMAG-Designer14.1 (JSOL Crop.) using the SRM model shown in the previous section.

In the simulation model of Fig. 9, the SRM is driven by a three-phase H-bridge inverter. This inverter is also lossless because the switching devices, as well as the DC power source, are all ideal. The DC voltage was set at 96 V, which was determined after the maximum voltage of the original SRM shown in Table I.

### A. Ripple Evaluation at Low Speed Small Torque Output

The input current and torque ripples are evaluated at comparatively low rotational speed and the low output torque, under which condition the phase current waveforms can be well controlled by the inverter and the magnetic saturation scarcely occurs in the SRM. The rotational speed was set at 500 r/min; the output torque was set at 1 N·m.

Figure 10 shows the simulation results. As can be seen in Fig. 10(a), the phase current waveform of the proposed technique successfully reduced the effective value by 18 % compared with the previous technique with the original rotor shape, which corresponds to the reduction of the copper loss by 33 %.

Furthermore, Fig. 10(b) and Fig. 10(c) indicate that the proposed technique successfully reduced both the input current and torque ripples compared with the conventional square-shaped phase current waveform with the original rotor shape, similarly as the previous technique with the original rotor shape. Torque ripple ratios of the proposed technique, the previous technique, and the conventional square-shaped phase current

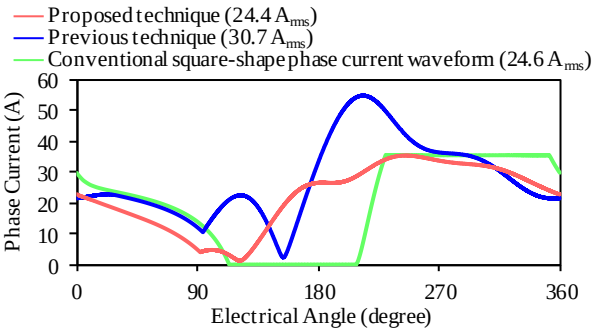


(a) Phase current waveform

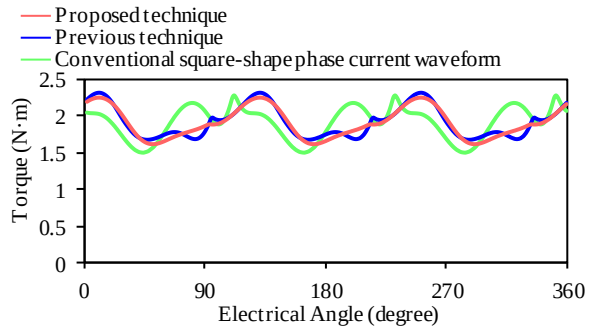


(b) Torque waveform

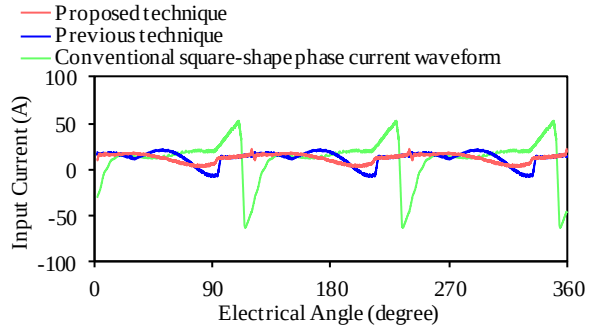


(c) Input current waveform

Fig. 11. Simulation result of the SRM operated at the rotational speed of 6000 r/min and the output torque of 1.9 N·m. The effective values of the phase current are presented in the legend of Fig. 11(a).

waveform were 11 %, 10 %, and 23 %, respectively. The input current ripple ratios of the proposed technique, the previous technique, and the conventional square-shaped phase current waveform were 217 %, 217 %, and 1924 %, respectively.

### *B. Ripple Evaluation at Rated Operation*

Next, the input current and torque ripples are evaluated at the rated operation of the SRM under consideration. The rated operation is specified in Table I as 1.2 kW and 6000 r/min, which indicates the torque output of 1.9 N·m.

Figure 11 shows the simulation results. As can be seen in the figure, the torque ripple of the proposed technique was almost the same as those of the previous technique and the conventional square-shaped phase current waveform. The torque ripple ratios of the proposed technique, previous technique, and the square-shaped phase current waveform were 17 %, 17 %, and 20 %, respectively.

Meanwhile, the proposed technique exhibited great reduction of the input current ripple, similarly as the previous technique,

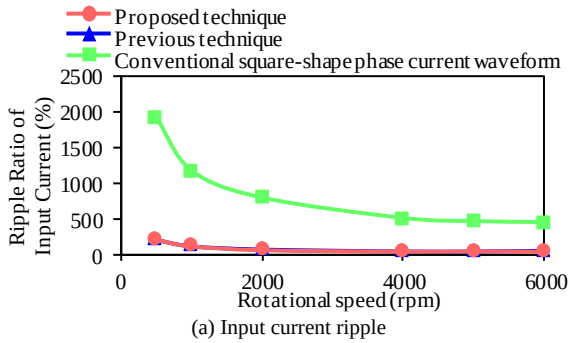


(a) Input current ripple

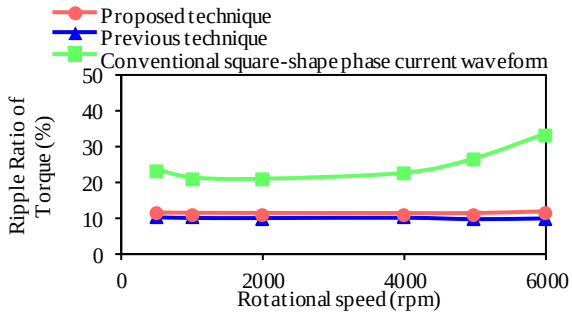


(b) Torque ripple

Fig. 12. Dependence of the input current ripple and the torque ripple on the rotational speed at the torque output of 1 N·m.

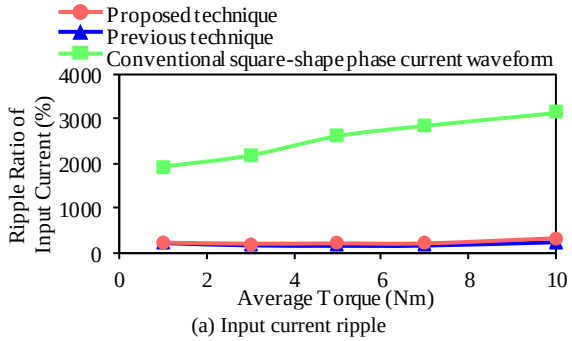


(a) Input current ripple

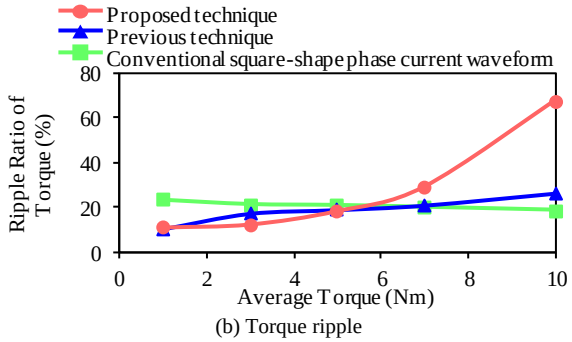


(b) Torque ripple

Fig. 13. Dependence of the input current ripple and the torque ripple on the average torque at the rotational speed of 500 r/min.

compared with the conventional square-shaped phase current. The input current ripple ratios of the proposed technique, previous technique, and the square-shaped phase current waveform were 81 %, 121 %, and 453 %, respectively.

The proposed technique reduced the effective value of the phase current waveform by 21 % compared with the previous technique, which corresponds to the reduction of the copper loss by 37 %.

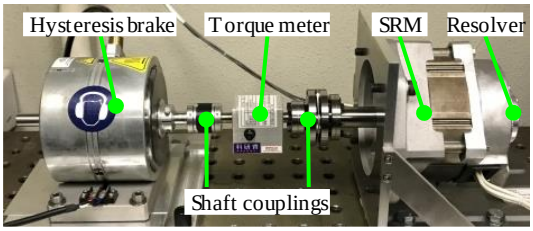


(a) Motor test bench employed for the experiment

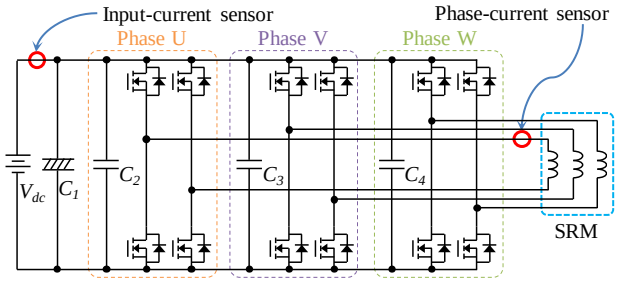


DC power supply ($V_{dc}$): GPO250-20R (Takasago)
Power MOS-FETs: IRFP4668PBF (International Rectifier)
$C_1$: LQR2W562MSEJ (5.6 mF, Nichicon) × 2
$C_2$, $C_3$, $C_4$: C4AEGBW6100A3NJ (100 μF, KEMET)
CKG57NX7T2W225M500JH (TDK) × 2

(b) Schematic diagram of the three-phase H-bridge inverter employed for driving the SRM

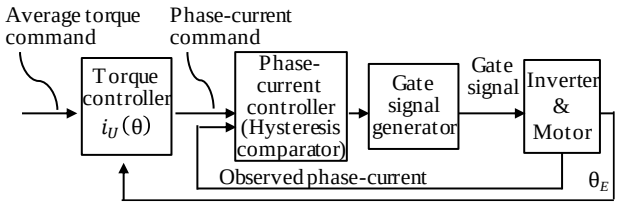


(c) Control diagram of the inverter

Fig. 14. Experimental set-up.

TABLE VI
SPECIFICATIONS OF MOTOR TEST BENCH

| Instrument | Specifications |
|---|---|
| SRM | RB165SR-96CSRM<br>(Motion System Tech. Inc.)<br>1.2 kW, 96 V, 6000 rpm<br>Stator: 12 poles, Rotor: 8 poles.<br>Number of turns: 14 turns/pole |
| Resolver | TS2224N1114E102<br>(Tamagawa Seiki Co., Ltd.) |
| Torque meter | UTMII-5Nm (Unipulse Corp.) |
| Shaft couplings | UCM65-12*24M, UCM34-12*12G<br>(Unipulse Corp.) |
| Hysteresis brake | AHB-6 (Magtrol Inc.) |

### C. *Ripple Evaluation at High Speed Operation*

Because this technique is intended to be applied to the vehicular propulsion, the operation is required to cover a wide range of the rotational speed as well as the output torque. This subsection investigated the input current and torque ripples at high rotational speed from 500 r/min to 6000 r/min, where the phase current began to deviate from the command value due to the limited DC bus voltage. The output torque was set at 1 N·m.

Figure 12 presents the input current ripple ratio and the torque ripple ratio of the proposed technique, the previous technique with the original rotor shape, and the conventional square-shaped phase current waveform with the original rotor shape. As can be seen in the figure, the proposed technique and the previous technique exhibited small input current and torque ripples at higher rotational speed than the conventional square-shaped phase current waveform. This result is consistent with the magnetic flux waveform shown in Fig. 4, in which both of the proposed technique and the previous technique showed far smoother magnetic flux waveform than the conventional square-shaped phase current waveform. Consequently, the simultaneous tuning of the rotor shape and the phase current waveform can reduce these two ripples at high rotational speed similarly as the previous technique.

### D. *Ripple Evaluation at Large Torque Output*

Next, the input current and torque ripples were investigated for wide output torque range from 1 N·m to 10 N·m, where the magnetic saturation affects the performance as the output torque increases. The rotational speed was set at 500 r/min.

Figure 13 presents the input current ripple ratio and the torque ripple ratio of the proposed technique, the previous technique with the original rotor shape, and the conventional square-shaped phase current waveform with the original rotor shape. As can be seen in the figure, the proposed technique and the previous technique exhibited small input current and torque ripples below the output torque of 5 N·m, although the proposed technique exhibited large torque ripple at the output torque higher than 5 N·m. This indicates that the tuning of the rotor shape and the phase current waveform resulted in greater susceptibility to the magnetic saturation, which should be solved in the future research. Nonetheless, the proposed technique exhibited small input current and torque ripples in a wide torque range.

To summarize the simulation results, simultaneous tuning of the rotor shape and the phase current waveform can reduce the two ripples with smaller effective value of the phase current than the previous technique, and reduction of these ripples can cover at high rotational speed, similarly as the previous technique. However, in the operation with extremely large torque output, the torque ripple can increase more than the previous technique due to the magnetic saturation.

## V. EXPERIMENT

Next, the experiment was carried out to verify the effectiveness of the tuning result of the rotor shape and the phase current waveform. Similarly as in the previous section, the experiment compared the effective value of the phase current, as well as the input current and torque ripples, of the tuned phase current waveform with the tuned rotor shape, i.e. the proposed technique, with the two phase current waveforms with the original rotor shape, i.e. the conventional square-shaped phase current waveform and the previous technique, in which only the phase current was tuned based on the original rotor shape.

Figure 14 depicts the experimental set-up employed for the experiment. Figure 14(a) is the photograph of the motor test bench. In this bench, an SRM and a hysteresis brake are connected mechanically via an instantaneous torque meter and

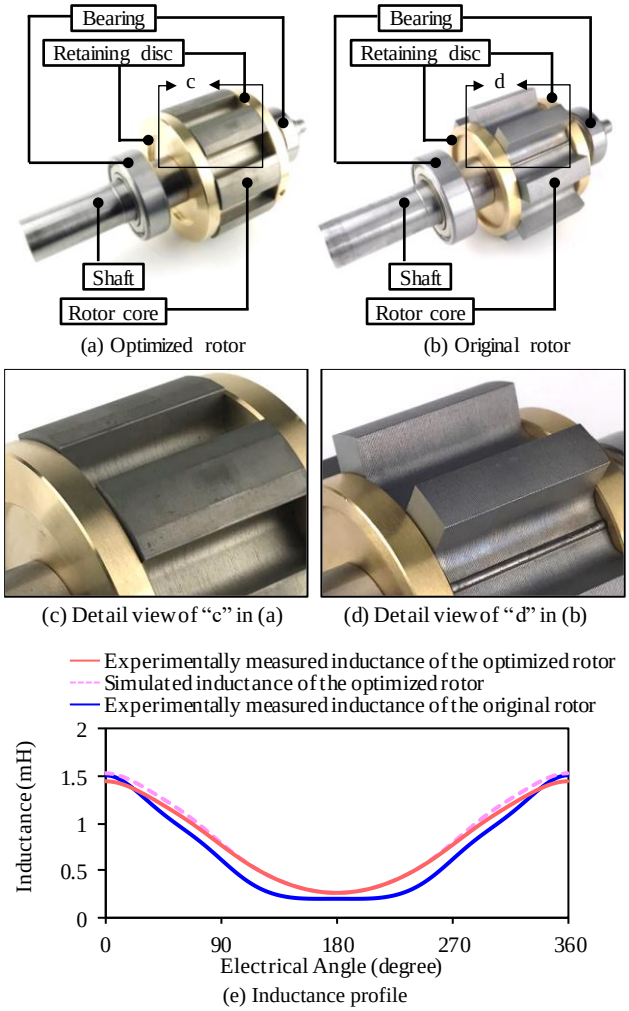

(a) Optimized rotor (b) Original rotor

(c) Detail view of "c" in (a) (d) Detail view of "d" in (b)

(e) Inductance profile

Fig. 15. Experimental rotors.

shaft couplings. The specifications of this motor test bench are listed in Table VI. (The specifications of the SRM is the same as Table I.) The rotational speed was controlled by adjusting the load torque of the hysteresis brake. Figure 14(b) illustrates the schematic diagram of the three-phase H-bridge inverter that drives the experimental SRM. The DC bus voltage $V_{dc}$ was set at 96 V, which was determined after the maximum voltage shown in Table I. This inverter controls the phase current of the experimental SRM to follow the predetermined phase current waveform according to the control diagram shown in Fig. 14(c). This control is a well-known basic inverter control method known as the hysteresis controller. The hysteresis width was set at 1.5A. The average switching frequency of the inverter was 28 kHz for the proposed technique, 30kHz for the previous technique, and 29 kHz for the conventional square-shaped phase current waveform, respectively. The overall control was implemented on a commercially available DSP platform. This experiment utilized PE-Expert 3 (Myway Corp.).

As this experiment uses two types of the rotor shapes, the following two rotors were constructed: The original rotor of the experimental SRM, which has a typical structure as a commercially available SRM as shown in Fig. 8(b), and the tuned rotor, which has the rotor shape shown in Fig. 8(a). Figure 15 presents the photographs of these rotors used in the experiment. These rotors share the same stator of the test bench. In the evaluation of the conventional square-shaped phase current waveform and the previous technique, the original rotor was inserted in the experimental SRM. Meanwhile, in the evaluation of the proposed technique, the tuned rotor was inserted in the experimental SRM. The tuned rotor exhibited almost the same inductance profile as the FEM analysis result shown in Fig. 6.

In this experiment, the SRM was operated at 1 N·m torque output and evaluated the performance at two rotational speed: 75 r/min and 3000 r/min. The rotational speed of 75 r/min was mainly for the measurement of the torque ripple. Because the instantaneous torque meter has the frequency limitation of approximately 1 kHz and the mechanical resonance of the motor test bench at approximately 125 Hz should be avoided from excitation, the torque ripple was measured at this extremely low rotation speed so that the harmonics were measured but could not excite the mechanical resonance in the test bench. Therefore, the torque and the input current were measured at 75 r/min, whereas only the input current was measured at 3000 r/min. On the other hand, because of the low efficiency at the extremely low rotational speed, the input current ripple may be affected by the copper loss at 75 r/min, which was not considered in the theory in the tuning procedure. Therefore, reduction of the input current ripple is expected to be more effective at 3000 r/min. As can be seen in [41][42], the rotational speed of 3000 r/min is one of the typical rotational speeds of the propulsion motors of the electric vehicles in the JC08 driving cycle and the new European driving cycle.

Figures 16 and 17 present the experimental results at 75 r/min and 3000 r/min, respectively. The effective values of the phase current are also presented in Fig. 16(a) and Fig. 17(a).

The phase current of the proposed technique successfully reduced the effective value by 23 % at 75 r/min, which corresponds to the reduction in the copper loss by 40 %, and by 12 % at 3000 r/min , which corresponds to the reduction in the copper loss by 22 %, compared with the previous technique. In spite of this effective reduction of the effective value, the phase current of the proposed technique has still higher effective value than the conventional square-shaped phase current waveform by 22 % at 75 r/min and by 21 % at 3000 r/min. Unlike the square-shaped phase current waveform, the phase current of the proposed technique well followed its command value at the rotational speed of 3000 r/min, as was expected from the simulation.

The proposed technique exhibited remarkable reduction in the torque ripple compared with the conventional square-shaped phase current waveform, similarly as the previous technique. As can be seen in Fig. 16(b), the torque ripple ratios at 75 r/min of the proposed technique, the previous technique, and the conventional square-shaped waveform were 9 %, 33 %, and 55 %, respectively.

The proposed technique also exhibited remarkable reduction in the input current ripple compared with the conventional square-shaped phase current waveform, similarly as the

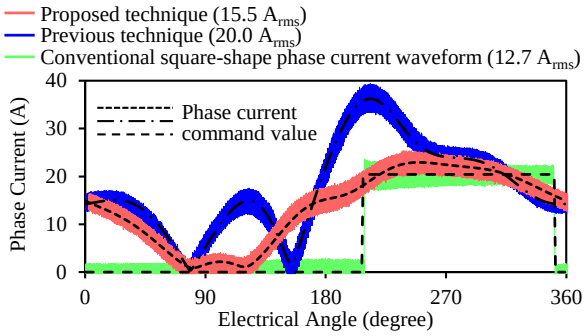


(a) Phase current waveform

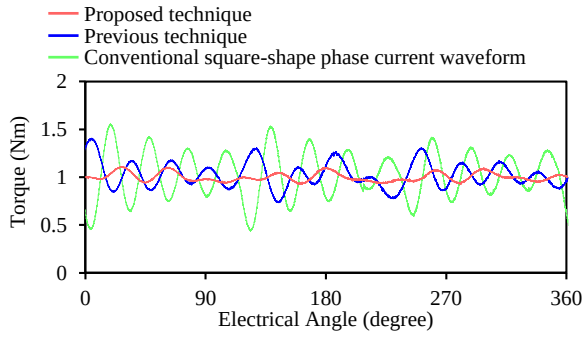


(b) torque waveform

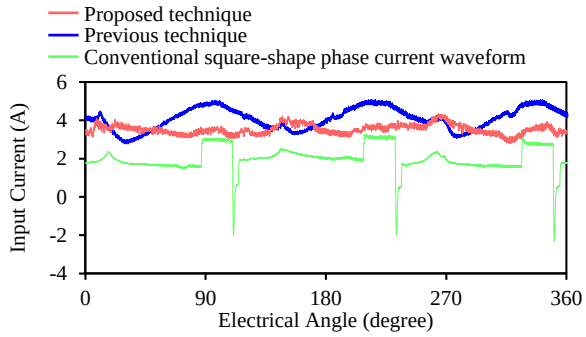


(c) Input current waveform

Fig. 16. Experimental result at the rotational speed of 75 r/min and the output torque of 1 N·m. The effective values of the phase current are presented in the legend of Fig. 16(a).

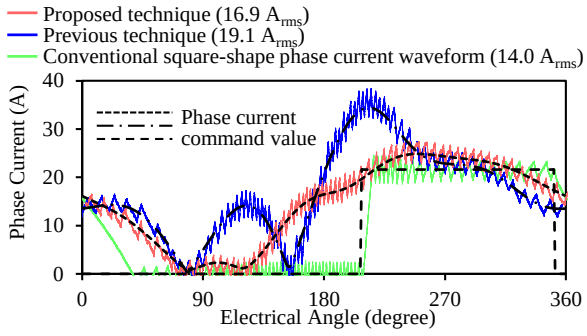


(a) Phase current waveform

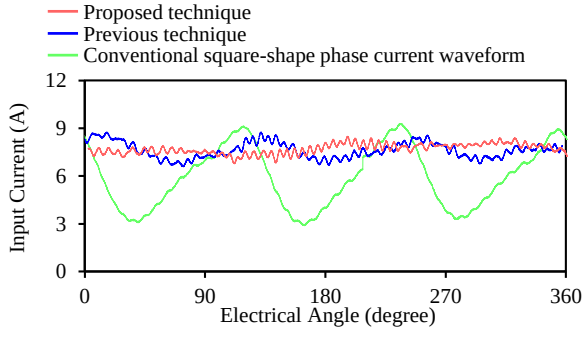


(b) Input current waveform

Fig. 17. Experimental result at the rotational speed of 3000 r/min and the output torque of 1 N·m. The effective values of the phase current are presented in the legend of Fig. 17(a).

previous technique. The input current ripple ratios at 75 r/min of the proposed technique, the previous technique, and the conventional square-shaped waveform were 22 %, 28 %, and 140 %, respectively. In addition, the input current ripple ratios at 3000 r/min of the proposed technique, the previous technique, and the conventional square-shaped waveform were 11 %, 33 %, and 54 %, respectively, supporting the effective reduction of the input current ripple for wide rotational speed, as was expected from the simulation.

Certainly, the input current ripple of the simulation was far greater than the experiment. The reason may lie in the power loss which was not considered in the simulation. The simulation result presented in Fig. 10 and Fig. 13 are the input current ripple at 500 r/min. At this low rotational speed, the DC current level of the input current is extremely small due to the small kinetic power output in the simulation. On the other hand, the actual motor bench generates the significant power loss even under the low kinetic power output, which increases the DC current level of the input current and reduces the input current ripple ratio. Furthermore, the experiment utilized the input smoothing capacitors to decouple the high frequency current ripple caused by the inverter switching to measure the low frequency input current ripple caused by the SRM operation. However, a part of the low frequency input current ripple may be decoupled by these input smoothing capacitors, which may have led to the decrease in the input current ripple in the experiment. On the other hand, the simulation result of the input current ripple in Fig. 10 still contains the high frequency ripple caused by the inverter switching, which may have led to the increase in the input current ripple in the simulation.

Nonetheless, the experiment successfully revealed that the proposed technique can successfully reduce the input current and torque ripples with reduced effective value of the phase current, which supports the effectiveness of the simultaneous tuning of the rotor shape and the phase current waveform.

## VI. Conclusions

The SRM is a promising motor for vehicular propulsion. However, the SRM tends to suffer from large input current ripple and large torque ripple, which are hindering application of the vehicular propulsion. Although the recently-proposed previous technique derived the phase current waveform that can simultaneously eliminate the input current and torque ripples, this phase current waveform tends to generate large copper loss when applied to many commercially available SRMs. To solve this problem, this paper proposed simultaneous tuning of the rotor shape and the phase current waveform, which can eliminate both of the input current and torque ripples with minimum effective value of the phase current. The simulation

and the experiment confirmed elimination of these two ripples with reduced effective value of the phase current compared with this previous technique, supporting effectiveness of simultaneous tuning of the rotor shape and the phase current waveform for applying SRMs to vehicular propulsion.

Despite the effectiveness of the proposed method, the proposed technique still exhibited larger effective value of the phase current than the conventional square-shaped phase current waveform. However, the tuning method of this paper does not indicate the global optimization. Therefore, there may remain the possibility of further reduction of the effective value of the phase current by future improvement in the simultaneous tuning method of the rotor shape and the phase current waveform.

## REFERENCES


[1] Z. Q. Zhu and C. C. Chan, "Electrical machine topologies and technologies for electric, hybrid, and fuel cell vehicles," in *Proc. IEEE Vehicle Power Propulsion Conf.*, Harbin, China, pp. 1–6, Sept. 2008.

[2] W. Suppharangsan and J. Wang, "Experimental validation of a new switching technique for DC-link capacitor minimization in switched reluctance machine drives," in *Proc. IEEE Int. Electric Machines Drives Conf.*, Chicago, USA, pp. 1031–1036, May 2013.

[3] I. Husain and M. Ehsani, "Torque ripple minimization in switched reluctance motor drives by PWM current control," *IEEE Trans. Power Electron.*, vol. 11, no. 1, pp. 83-88, Jan. 1996.

[4] M. Rodrigues, P. J. Costa Branco, and W. Suemitsu, "Fuzzy logic torque ripple reduction by turn-off angle compensation for switched reluctance motors," *IEEE Trans. Ind. Electron.*, vol. 48, no. 3, pp. 711-715, June 2001.

[5] I. Husain, "Minimization of torque ripple in SRM drives," *IEEE Trans. Ind. Electron.*, vol. 49, no. 1, pp. 28-39, Feb. 2002.

[6] L. O. A. P. Henriques, P. J. Costa Branco, L. G. B. Rolim, and W. I. Suemitsu, "Proposition of an offline learning current modulation for torque-ripple reduction in switched reluctance motors: design and experimental evaluation," *IEEE Trans. Ind. Electron.*, vol. 49, no. 3, pp. 665-676, June 2002.

[7] A. D. Cheok and Y. Fukuda, "A new torque and flux control method for switched reluctance motor drives," *IEEE Trans. Power Electron.*, vol. 17, no. 4, pp. 543-557, Jul. 2002.

[8] P. L. Chapman and S. D. Sudhoff, "Design and precise realization of optimized current waveforms for an 8/6 switched reluctance drive," *IEEE Trans. Power Electron.*, vol. 17, no. 1, pp. 76-83, Jan. 2002.

[9] C. Mademlis and I. Kioskeridis, "Performance optimization in switched reluctance motor drives with online commutation angle control," IEEE Trans. Energy Conversion, vol. 18, no. 3, pp. 448-457, Sept. 2003.

[10] A. M. Omekanda, "A new technique for multidimensional performance optimization of switched reluctance motors for vehicle propulsion," *IEEE Trans. Ind. Appl.*, vol. 39, no. 3, pp. 672-676, May 2003.

[11] N. T. Shaked and R. Rabinovici, "New procedures for minimizing the torque ripple in switched reluctance motors by optimizing the phase-current profile," *IEEE Trans. Magn.*, vol. 41, no. 3, pp. 1184-1192, Mar. 2005.

[12] Y. Sozer and D. A. Torrey, "Optimal turn-off angle control in the face of automatic turn-on angle control for switched-reluctance motors," *IET Electric Power Appl.*, vol. 1, no. 3, pp. 395-401, May 2007.

[13] X. D. Xue, K. W. E. Cheng, and S. L. Ho, "Optimization and evaluation of torque-sharing functions for torque ripple minimization in switched reluctance motor drives," *IEEE Trans. Power Electron.*, vol. 24, no. 9, pp. 2076-2090, Sept. 2009.

[14] D. H. Lee, J. Liang, Z. G. Lee, and J. W. Ahn, "A simple nonlinear logical torque sharing function for low-torque ripple SR drive," *IEEE Trans. Ind. Electron.*, vol. 56, no. 8, pp. 3021 – 3028, Aug. 2009.

[15] X. D. Xue, K. W. E. Cheng, J. K. Lin, Z. Zhang, K. F. Luk, T. W. Ng, and N. C. Cheung, "Optimal control method of motoring operation for srm drives in electric vehicles," *IEEE Trans. Vehicular Tech.*, vol. 59, no. 3, pp. 1191-1204, Mar. 2010.

[16] V. P. Vujičić, "Minimization of torque ripple and copper losses in switched reluctance drive," *IEEE Trans. Power Electron.*, vol. 27, no. 8, pp. 388-399, Jan. 2012.

[17] C. Moron, A. Garcia, E. Tremps, and J. A. Somolinos, "Torque control of switched reluctance motors," *IEEE Trans. Magn.*, vol. 48, no. 4, pp. 1661-1664, Apr. 2012.

[18] J. Ye, B. Bilgin, and A. Emadi, "An offline torque sharing function for torque ripple reduction in switched reluctance motor drives," *IEEE Trans. Energy Conversion*, vol. 30, no. 2, pp. 726-735, June 2015.

[19] J. Ye, B. Bilgin, and A. Emadi, "An extended-speed low-ripple torque control of switched reluctance motor drives," *IEEE Trans. Power Electron.*, vol. 30, no. 3, pp. 1457-1470, Mar. 2015.

[20] P. Dúbravka, P. Rafajdus, P. Makyš, and L. Szabó, "Control of switched reluctance motor by current profiling under normal and open phase operating condition," *IET Electric Power Appl.*, vol. 11, no. 4, pp. 548-556, Apr. 2017.

[21] H. Li, B. Bilgin, and A. Emadi, "An improved torque sharing function for torque ripple reduction in switched reluctance machines," *IEEE Trans. Power Electron.*, vol. 34, no. 2, pp. 1635-1644, Feb. 2019.

[22] T. Husain, A. Elrayyah, Y. Sozer, and I. Husain, "Unified control for switched reluctance motors for wide speed operation," *IEEE Trans. Ind. Electron.*, vol. 66, no. 5, pp. 3401-3411, May 2019.

[23] M. Kawa, K. Kiyota, J. Furqani, and A. Chiba, "Acoustic noise reduction of a high-efficiency switched reluctance motor for hybrid electric vehicles with novel current waveform," *IEEE Trans. Ind. Appl.*, vol. 55, no. 3, pp. 2519-2528, May 2019.

[24] N. K. Sheth and K. R. Rajagopal, "Optimum pole arcs for a switched reluctance motor for higher torque with reduced ripple," *IEEE Trans. Magn.*, vol. 39, no. 5, pp. 3214-3216, Sept. 2003.

[25] J. W. Lee, H. S. Kim, B. I. Kwon, and B. T. Kim, "New rotor shape design for minimum torque ripple of SRM using FEM," *IEEE Trans. Magn.*, vol. 40, no. 2, pp. 754-757, Mar. 2004.

[26] N. K. Sheth and K. R. Rajagopal, "Torque profiles of a switched reluctance motor having special pole face shapes and asymmetric stator poles," *IEEE Trans. Magn.*, vol. 40, no. 4, pp. 2035-2037, Jul. 2004.

[27] Y. K. Choi, H. S. Yoon, and C. S. Koh, "Pole-shape optimization of a switched-reluctance motor for torque ripple reduction," *IEEE Trans. Magn.*, vol. 43, no. 4, pp. 1797-1800, Apr. 2007.

[28] X. D. Xue, K. W. E. Cheng, T. W. Ng, and N. C. Cheung, "Multi-objective optimization design of in-wheel switched reluctance motors in electric vehicles," *IEEE Trans. Ind. Electron.*, vol. 57, no. 9, pp. 2980-2987, Sept. 2010.

[29] G. Li, J. Ojeda, S. Hlioui, E. Hoang, M. Lecrivain, and M. Gabsi, "Modification in rotor pole geometry of mutually coupled switched reluctance machine for torque ripple mitigating," *IEEE Trans. Magn.*, vol. 48, no. 6, pp. 2025-2034, June 2012.

[30] R. Mikail, I. Husain, Y. Sozer, M. S. Islam, and T. Sebastian, "Torque-ripple minimization of switched reluctance machines through current profiling," *IEEE Trans. Ind. Appl.*, vol. 49, no. 3, pp. 1258-1267, May 2013.

[31] H. U. Shin and K. B. Lee, "Optimal design of a 1 kW switched reluctance generator for wind power systems using a genetic algorithm," *IET Electric Power Appl.*, vol. 10, no. 8, pp. 807-817, Sept 2016.

[32] J. Zhu, K. W. E. Cheng, X. Xue, and Y. Zou, "Design of a new enhanced torque in-wheel switched reluctance motor with divided teeth for electric vehicles," *IEEE Trans. Magn.*, vol. 53, no. 11, Nov. 2017, Art. no. 2501504.
[33] B. Anvari, H. A. Toliyat, and B. Fahimi, "Simultaneous optimization of geometry and firing angles for in-wheel switched reluctance motor drive," *IEEE Trans. Transportation Electrification*, vol. 4, no. 1, pp. 322-329, Mar. 2018.
[34] C. R. Neuhaus, N. H. Fuengwarodsakul, and R. W. De Doncker, "Control scheme for switched reluctance drives with minimized DC-link capacitance," *IEEE Trans. Power Electron.*, vol. 23, no. 5, pp. 2557-2564, Sept. 2008.
[35] W. Suppharangsan, and J. Wang, "Switching technique for minimisation of DC-link capacitance in switched reluctance machine drives," *IET Elect. Syst. Transportation*, vol. 5, no. 4, pp. 185-193, Dec. 2015.
[36] F. Yi and W. Cai, "A quasi-Z-source integrated multiport power converter as switched reluctance motor drives for capacitance reduction and wide-speed-range operation," *IEEE Trans. Power Electron.*, vol. 31, no. 11, pp. 7661-7676, Nov. 2016.
[37] W. Cai and F. Yi, "An integrated multiport power converter with small capacitance requirement for switched reluctance motor drive," *IEEE Trans. Power Electron.*, vol. 31, no. 4, pp. 3016-3026, Apr. 2016.
[38] F. Yi and W. Cai, "Modeling, control, and seamless transition of the bidirectional battery-driven switched reluctance motor/generator drive based on integrated multiport power converter for electric vehicle," *IEEE Trans. Power Electron.*, vol. 31, no. 10, pp. 7099-7111, Oct. 2016.
[39] T. Kusumi, T. Hara, K. Umetani, and E. Hiraki, "Simple control technique to eliminate source current ripple and torque ripple of switched reluctance motors for electric vehicle propulsion," in *Proc. Annu. Conf. IEEE Ind.l Elect. Soc. (IECON2016)*, Florence, Italy, pp. 1876-1881, Oct. 2016.
[40] T. Kusumi, T. Hara, K. Umetani, and E. Hiraki, "Simple analytical derivation of magnetic flux profile eliminating source current ripple and torque ripple of switched reluctance motors for electric vehicle propulsion," in *Proc. IEEE Appl. Power Electron. Conf. Expo. (APEC2017)*, Tampa, FL, USA, pp. 3142-3149, Mar. 2017.
[41] Y. Miyama, M. Hazeyama, S. Hanioka, A. Daikoku, and M. Inoue, "PWM carrier harmonic iron loss reduction technique of permanent-magnet motors for electric vehicles," IEEE Trans. Ind. Electron., vol. 52, no. 4, pp. 2865-2871, Jul./Aug. 2016.
[42] H.-J. Park and M.-S. Lim, "Design of high power density and high efficiency wound-field synchronous motor for electric vehicle traction," IEEE Access, vol. 7, pp. 46677-46685, Mar. 2019.
[43] T. Kusumi, T. Hara, K. Umetani, and E. Hiraki, "Rotor configuration which reduces copper loss of switched reluctance motors with suppression of torque ripple and input current ripple," in *Proc. IEEE Energy Conversion Congr. Expo. (ECCE2018)*, Portland, OR, USA, pp. 6097-6103, Sept. 2018.
[44] T. Hara, T. Kusumi, K. Umetani, and E. Hiraki, "A simple behavior model for switched reluctance motors based on magnetic energy," in *Proc. Intl. Power Electron. Motion Ctrl. Conf. (IPEMC2016)*, Hefei, China, May. 2016.

**Takayuki Kusumi** (S'17) was born in Okayama, Japan. He received the B. and M. degrees in electrical engineering from Okayama University, Okayama, Japan, in 2015 and 2017, respectively.

He is currently a Ph. D. student of Graduated School of Natural Science and Technology, Okayama University, Okayama, Japan. His research interest includes control technique for switched reluctance motors.

Mr. Kusumi is a member of the Institute of Electrical Engineers of Japan.

**Takuto Hara** was born in Kagawa, Japan. He received the B. and M. degrees in electrical engineering from Okayama University, Okayama, Japan, in 2016 and 2018, respectively.

He is currently an engineer for FUJI ELECTRIC CO., LTD., Mie, Japan. His research interest includes behavior model of switched reluctance motors.

**Kazuhiro Umetani** (M'12) was born in Kobe, Japan. He received the M. and Ph. D. degree in geophysical fluid dynamics from Kyoto University, Kyoto, Japan in 2004 and 2007, respectively. In 2015, he received the second Ph. D. degree in electrical engineering from Shimane University, Japan.

From 2007 to 2008, he was a Circuit Design Engineer for Toshiba Corporation, Japan. From 2008 to 2014, he was with the Power Electronics Group in DENSO CORPORATION, Japan. From 2014 to 2020, he was an Assistant Professor at Okayama University, Okayama, Japan. He is currently an Associate Professor at Tohoku University, Miyagi, Japan. His research interests include new circuit configurations in power electronics and power magnetics for vehicular applications.

Dr. Umetani is a member of the Institute of Electrical Engineers of Japan and the Japan Institute of Power Electronics.

**Eiji Hiraki** (M'03) was born in Yamaguchi, Japan. He received the M.Sc. and Ph.D. degrees from Osaka University, Osaka, Japan, in 1990 and 2004, respectively.

He joined Mazda Motor Corporation in 1990. From 1995 to 2013, he was with the Power Electronics Laboratory, Yamaguchi University, Yamaguchi, Japan. He is currently a Professor with the Electric Power Conversion System Engineering Laboratory, Okayama University, Okayama, Japan. His research interests include circuits and control systems of power electronics, particularly soft-switching technique for high-frequency switching power conversion systems.

Dr. Hiraki is a member of the Institute of Electrical Engineers of Japan and the Japan Institute of Power Electronics.